AO 9544 Aeolus + Innovation

SEA-FLECT:

Winds from Aeolus LIDAR

SEA Surface ReFLECTance

Delivery D4

Level 2 Surface Wind speed Product Algorithmic Theoretical Baseline Document

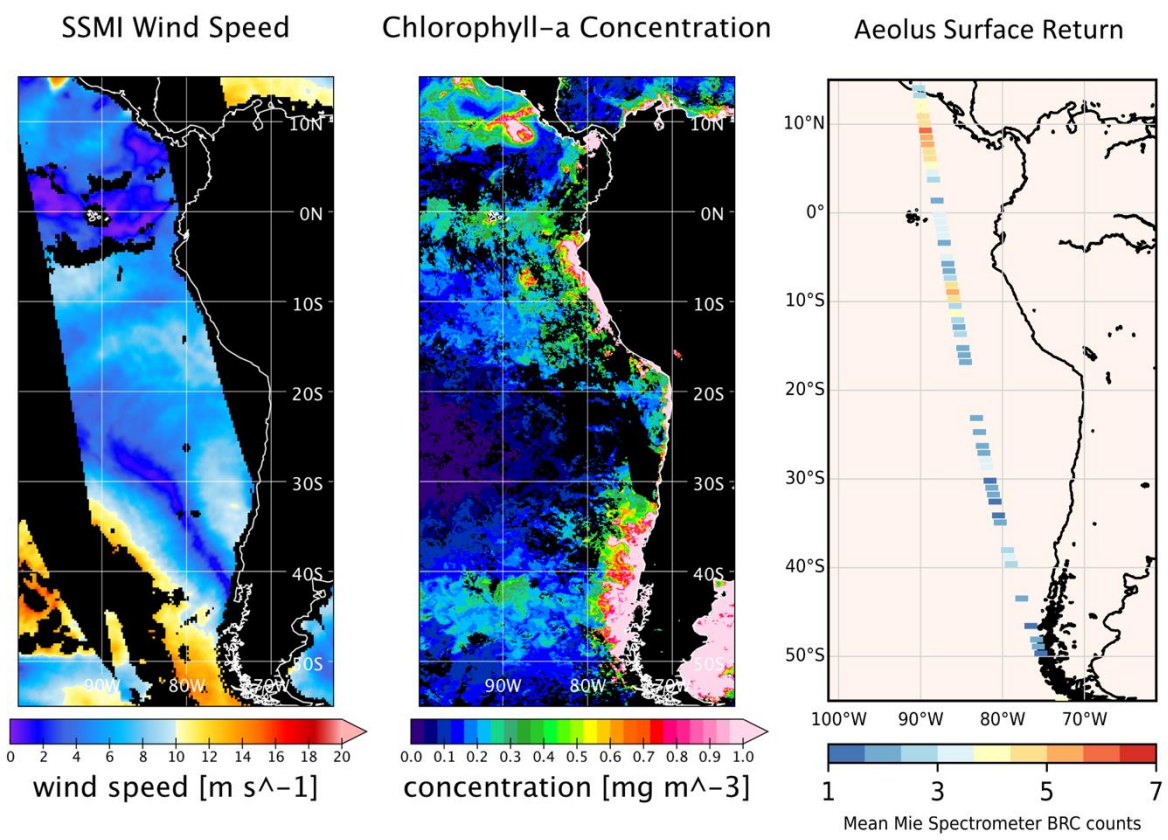

Doc. No.:	AERD/P2466/ESA/AO9544/D4	
Issue. No.:	0	
Version:	1.0.0	
Date:	27 October 2021	
Document prepared under ESA Contract Number: 4000133131/20/I-BG		

Table of contents

1 INTRODUCTION

1.1 Aeolus-ADM Aeolus mission

The Atmospheric Laser Doppler Instrument (ALADIN) is a High Spectral Resolution backscatter LIDAR (Light detecting and Ranging) instrument operating at a wavelength of 355 nm (ultra-violet). It is the mission payload of the Aeolus Atmospheric Dynamics Mission (ADM-Aeolus) as part of the ESA Earth Explorer Programme. The launch date of the Aeolus satellite was 22 August 2018. The primary mission objective is to demonstrate, from space, the measurement of wind profiles higher up in the atmosphere, in order to improve atmospheric weather model analyses and forecasts of the 3D vector winds. Details on the mission and the systems can be found in the Mission Requirements Document [MRD] and System Requirements Document [SRD], respectively.

1.2 Sea-Flect Study objective

The standard Aeolus wind product (L2B) is derived from examining the Doppler shift in either the Rayleigh or Mie scattering instrument. The Doppler shift depends on the motion of molecules or aerosols. The ocean surface wind product as developed in this project will be derived as a function of the lidar reflections of the ocean surface, rather than the doppler shifts in the atmosphere.. In short, the main objective of SEA-FLECT study project is to define, calibrate and validate an ocean surface wind speed retrieval method from ALADIN lidar surface returns. The wider scientific context and ratinale are explained in the SEA-FLECT Science Requirements Baseline (SRB) Document.

1.3 Document objective and organisation

This Algorithmic Theoretical Baseline Document (ATBD) aims to describe in detail the applied algorithmic methods to retrieve surface wind product from the ALADIN lidar surface returns. It states the main underlying equations and includes the description, derivation, rationale and specification of the related variables and parameters.

Structure:

- Chapter 1: This introduction.
- Chapter 2: General background and approach
- Chapter 3: Description of the applied retrievals of Aeolus Sea surface reflectance (observations)
- Chapter4: Description of the applied Geophysical Model Function and Wind Inversion

Applicable and reference documents

[ASPD] Aeolus Sensor and Product Description, ESA Report, AE-SU-ESA-GS-000, version 1.1, 28-Oct-2018.

1.4 [ATBD-L2A] Flamant, P. et al.: ADM-Aeolus L2A Algorithm Theoretical Basis Document (ATBD), Particle spin-off products, Document number: AE-TN-IPSL-GS-001, Version 5.5, 17. Jan. 2017, javascript:openWindow('https://earth.esa.int/files/Aeolus_complete_documents_package'), 2017.

[ATBD-L1B] ADM-Aeolus Algorithm Theoretical Basis Document ATBD Level1B Products Oliver Reitebuch, Dorit Huber, Ines Nikolaus, DLR, AE-RP-DLR-L1B-001, version 4.4, 20.04.2018.

[CALVAL-REQ] ADM-Aeolus: Scientific Calibration and Validation Requirements ESA. Report AE-RS-ESA-GS-005, version 2.1, 2014.

[MRD] ADM-Aeolus Mission Requirements Document (MRD), version 2.0, ESA Mission Science Division report AE-RP-ESA-SY-001 EOP-SM/2047, 16-11-2016.

[TN-ECMWF] Aeolus Level-2B Algorithm Theoretical Basis Document (Mathematical Description of the Aeolus L2B Processor) Ref: AE-TN-ECMWF-L2BP-0023 Version: 3.2 14 February 2019.

[Cox and Munk 1954] C. Cox and W. Munk, "Measurement of the Roughness of the Sea Surface from Photographs of the Sun's Glitter," *J. Opt. Soc. Am.*, 44, 838-850, 1954.

[Flamant et al., 1998] Flamant, C., Trouillet, V., Chazette, P., and Pelon, J.: Wind speed dependence of atmospheric boundary layer optical properties and ocean surface reflectance as observed by airborne backscatter lidar, *J. Geophys. Res. Ocean*, 103, 25137–25158, https://doi.org/10.1029/98JC02284, 1998.

[Fouladinejad et al., 2019] Fouladinejad, F., Matkan, A., Hajeb, M., and Brakhasi, F.: History and Applications of Space-Borne Lidars, Int. Arch. Photogramm. Remote Sens. Spatial Inf. Sci., XLII-4/W18, 407–414, https://doi.org/10.5194/isprs-archives-XLII-4-W18-407-2019, 2019.

[Hu et al., 2008] Hu, Y., Stamnes, K., Vaughan, M., Pelon, J., Weimer, C., Wu, D., Cisewski, M., Sun, W., Yang, P., Lin, B., Omar, A., Flittner, D., Hostetler, C., Trepte, C., Winker, D., Gibson, G., and Santa-Maria, M.: Sea surface wind speed estimation from space-based lidar measurements, *Atmos. Chem. Phys.*, 8, 3593–3601, https://doi.org/10.5194/acp-8-3593-2008, 2008.

[Jamet et al., 2019] Jamet C, Ibrahim A, Ahmad Z, Angelini F, Babin M, Behrenfeld MJ, Boss E, Cairns B, Churnside J, Chowdhary J, Davis AB, Dionisi D, Duforêt-Gaurier L, Franz B, Frouin R, Gao M, Gray D, Hasekamp O, He X, Hostetler C, Kalashnikova OV, Knobelspiesse K, Lacour L, Loisel H, Martins V, Rehm E, Remer L, Sanhaj I, Stamnes K, Stamnes S, Victori S, Werdell J and Zhai P-W: Going Beyond Standard Ocean Color Observations: Lidar and Polarimetry. *Front. Mar. Sci.* 6:251, https://doi.org/10.3389/fmars.2019.00251, 2019.

[de Kloe and Stoffelen, 2008] J. de Kloe and A. Stoffelen: Technical note on Ocean Albedo as a function of local wind and wave conditions and its effect on the zero-wind calibration, KNMI report AE-TN-KNMI-L1B-001, version 1.0, 15 April 2008.

[Koepke, 1984] Koepke, P.: Effective Reflectance of Oceanic Whitecaps, *Applied Optics*, 23, 1816–1824, 1984.

[Li et. al. 2010] Li, Z., Ch. Lemmerz, U. Paffrath, O. Reitebuch, and B. Witschas: Airborne Doppler lidar Investigation of Sea Surface Reflectance at a 355-nm Ultraviolet Wavelength. J. *Atmos. Oceanic Tech.*, 693-704, 2010.

[Ligi et al., 2017] Martin Ligi, Tiit Kutser, Kari Kallio, Jenni Attila, Sampsa Koponen, Birgot Paavel, Tuuli Soomets, Anu Reinart: Testing the performance of empirical remote sensing algorithms in the Baltic Sea waters with modelled and in situ reflectance data, *Oceanologia*, 59 (1), 57-68, https://doi.org/10.1016/j.oceano.2016.08.002, 2017.

[Lux et al., 2018] Lux, O., Lemmerz, C., Weiler, F., Marksteiner, U., Witschas, B., Rahm, S., Schäfler, A., and Reitebuch, O.: Airborne wind lidar observations over the North Atlantic in 2016 for the pre-launch validation of the satellite mission Aeolus, *Atmos. Meas. Tech.*, 11, 3297–3322, https://doi.org/10.5194/amt-11-3297-2018, 2018.

[Lux et al., 2020] Lux, O., Lemmerz, C., Weiler, F., Marksteiner, U., Witschas, B., Rahm, S., Geiß, A., and Reitebuch, O.: Intercomparison of wind observations from the European Space Agency's Aeolus satellite mission and the ALADIN Airborne Demonstrator, *Atmos. Meas. Tech.*, 13, 2075–2097, https://doi.org/10.5194/amt-13-2075-2020, 2020.

[Menzies et al.,1998] Robert T. Menzies, David M. Tratt, and William H. Hunt: Lidar In-space Technology Experiment measurements of sea surface directional reflectance and the link to surface wind speed, *Appl. Opt.*, 37, 5550-5559, 1998.

[Monahan and O'Muircheartaigh, 1986] Monahan, E. C. and I. G. O'Muircheartaigh: Whitecaps and the passive remote sensing of the ocean surface, *Int. J. Remote Sensing*, 7, 627–642, 1986.

[Morel and Prieur, 1977] Morel, A. and Prieur, L.: Analysis of variations in ocean color, *Limnol. Oceanogr.* 22: 709-722, 1977.

[Morel et al., 2007] Morel, André, Gentili, Bernard, Claustre, Hervé, Babin, Marcel, Bricaud, Annick, Ras, Joséphine, Tièche, Fanny: Optical properties of the "clearest" natural waters, *Limnology and Oceanography*, 52, https://doi.org/10.4319/lo.2007.52.1.0217, 2017.

[Morel et al., 2007-b] Morel, A., Claustre, H., Antoine, D., and Gentili, B.: Natural variability of bio-optical properties in Case 1 waters: attenuation and reflectance within the visible and near-UV spectral domains, as observed in South Pacific and Mediterranean waters, *Biogeosciences*, 4, 913–925, https://doi.org/10.5194/bg-4-913-2007, 2007.

[Morel et al., 2010] Morel, A., Claustre, H., and Gentili, B.: The most oligotrophic subtropical zones of the global ocean: similarities and differences in terms of chlorophyll and yellow substance, *Biogeosciences*, 7, 3139–3151, https://doi.org/10.5194/bg-7-3139-2010, 2010.

[Straume, 2018] A. G. Straume, Aeolus Sensor and Product Description, ESA report AE-SU-ESA-GS-000. Oct 2018.

[Sun, 2018] Sun, X.: Lidar Sensors from Space. In: Comprehensive Remote Sensing, 412-434, Editor(s): Shunlin Liang, Elsevier, ISBN 9780128032213, https://doi.org/10.1016/B978-0-12-409548-9.10327-6, 2018.

[Tratt et al., 2002] Tratt, D. M., R. T. Menzies, M. P. Chiao, D. R. Cutten, J. Rothermel, R.M. Hardesty, J. N. Howell, and S. L. Durden, 2002: Airborne Doppler lidar investigation of the wind modulated sea-surface angular retroreflectance signature. *Appl. Opt.*, 33, 6941–6950.

[Tyler and Smith, 1970] Tyler, J.E., Smith, R.C., 1970. Measurements of spectral irradiance underwater. Gordon & Breach Publishing Group.

2 GENERAL THEORETICAL BACKGROUND AND APPROACH

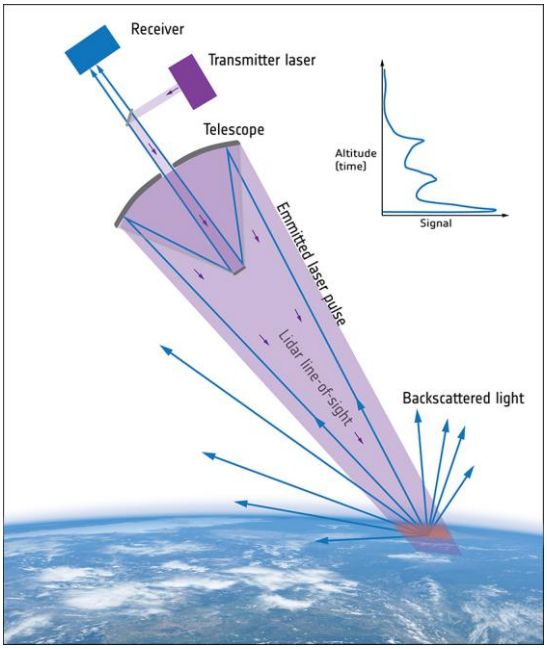

Figure 1 Sketch of the Lidar principle.

2.1 Lidar Equation

The received energy of the backscatter signal (see Figure 1) can be determined by the Lidar equation [ATBD-L1B]. This equation takes both instrumental parameters and atmospheric variables into account. The backscatter laser energy at a distance *r* from the lidar is given by:

$$E(\lambda,r) = E_L \cdot \Delta R / r^2 \cdot A_0 \cdot C(\lambda) \cdot \beta(\lambda,r) \cdot T^2(\lambda,r)$$

Equation 1: Lidar equation.

Λ	Laser wavelength (355 nm)
R	Distance from Lidar
$E(\lambda,r)$	Backscattered energy
E_L	Transmitted Pulse energy
ΔR	Range Resolution
A_0/r^2	Accepting solid angle. A_0 is the Optical Aperture
$\beta(\lambda,r)$	atmospheric backscatter coefficient $\beta(\lambda,r)$
$C(\lambda)$	Instrumental constant
$T^2(\lambda,r)$	transmission coefficient

2.2 Sea Surface refectivity

The atmospheric backscatter coefficient $\beta(\lambda,r)$ characterizes the illuminated atmospheric volume backscatter. For backscatter returns from the earth surface, the reflectance is provided in terms of an albedo which is the ratio of radiation reflected by the surface with the incident energy.

$$a = \beta(\lambda, r)\, \Delta R$$

Equation 2: Albedo.

This sometimes can be modelled as a constant. However, the reflectance of (ocean) water surfaces depends strongly on the incidence angle (nearly constant in this case) and is composed of three main contributions:

1. Specular reflection from the sea surface,
2. Lambertian or diffuse reflection from the sea surface, and
3. sub-surface reflection.

Menzies et al. [1998] expressed the total ocean water light reflectance as:

$$R = R_{wc} + (1 - W)R_s + (1 - R_{wc})R_U$$

Equation 3: Total surface reflectance.

R	Total reflectance	
R_s	Specular (surface) contribution	
$R_{wc} = W \cdot R_{wc,eff} \frac{\cos\theta}{\pi}$	Whitecap contribution	
$R_{wc,eff}$	Effective whitecap contribution	Constant
R_U	Subsurface (underwater) contribution	
θ	Off-nadir angle	Look angle
W	White caps coverage	Fraction

2.3 Wind retrieval

As can be seen from the total reflectance formula, the dependence on the wind speed U is complex and cannot be inverted analytically. Therefore, the windspeed is retrieved by minimizing the difference between the R_{obs}, the observed reflectivity derived from the sea surface return, and the modeled reflectance:

$$\min_U (R_{obs} - R(U))^2$$

Hence the overall retrieval of the observed wind speed consists of four main components:

1. **Observed surface reflectivity retrieval:** The extraction and assessment of the observed ocean surface reflectivity from the Aeolus observational products.
2. **Geophysical modelling:** The mathematical description of the three (see 3.2) components each approximating the contribution to the total modelled reflection This mathematical description will be called the Geophysical Model Function (GMF).
3. **Wind inversion:** Wind speed is retrieved by minimizing the difference between the R_{obs}, the observed reflectivity of the sea surface return, and the modelled reflectance.

4. **Product generation.**

3 OBSERVED SURFACE REFLECTIVITY

Observation Geometry

3.1

Aeolus is in a sun-synchronous orbit at a flight altitude of 320 km. The Lidar instrument ALADIN emits pulses orthogonally to the satellite ground-track, pointing 35° off-nadir, away from the sun (see **Error! Reference source not found.**). The ALADIN receiver then measures the radiation which has been back-scattered into the Lidar's line-of-sight (LOS), see Figure .

3.2 Horizontal resolution aspects

The retrieval has to take place at certain horizontal resolution. For calibration and validation purposes the Aeolus mission has introduced the so-called measurement scale and observation scale, see [CALVAL-REQ]. One measurement consists of the accumulation of 19 outgoing laser pulses resulting in a horizontal measurement sampling of about 3 km. Subsequent measurements are again averaged in groups of 30, resulting in a horizontal resolution of about 87 km for the wind observations.

3.3

Mie Measurement

The observed reflectivity, R_{obs}, is proportional to the Level 1B range corrected Mie signal intensity (ACCD counts * m^{-2}) [Lux et al., 2018, 2020] in the range bins that contains the sea surface, typically range bin 23. Because the relation between accumulated ACCD counts and surface reflectivity, R_{obs}, is not known *a priori*, a scaling between range corrected Mie signal intensity and modelled reflectivity, $R(U)$, and will need to be empirically derived.

The integration time over 7 seconds results in a spatial sampling scale of ~ 87 km. The integrated sea surface reflectivity over the 87 km will contain contributions from the three components described above in Section 2.3.3.2. But the contributions to reflectivity from aerosols and white capping are primarily dependent on the retrieved wind speed, U, while the subsurface reflection depends on ocean colour. So, the retrieved wind will represent the

average estimated wind along the 87 km sampling distance, assuming average reflectivities from whitecaps, aerosols and subsurface waters.

Pre-processing and filtering sensitivities

3.4.1 Cloud screening:

3.4 The Mie channel is very sensitive to clouds and aerosols. Mie channel returns from clouds are several orders of magnitude higher than from clear skies, and conversely, Mie channel SNR because of clouds is several orders of magnitude lower. Therefore, it is likely that joint examination of Mie channel returns and Mie channel SNR is a sufficiently accurate tool for cloud screening, removing the need for collocation with other sensor data to identify clouds. Simulated and flight data from Lux et al. [2018, 2020] demonstrate the sensitivity of Mie channel and Mie channel SNR to clouds and aerosols.

The other types of screening criteria discussed previously include:

- 'ocean colour' type: oligotrophic, case II, …
- 'sea state' type: wind sea, swell, anisotropy,
- wind speed type: low wind, moderate wind, (very) high wind,
- 'Lidar bin condition' type: filtering on the fraction of the range bin that contains atmosphere/ocean.

The screening criteria and filtering will be part of the versioning mentioned in the cal/val section 5

The aerosols in the atmosphere portion of the surface range bin may provide enhanced backscatter. From the Mie measurements of Aeolus, estimates of the backscatter coefficient, β, and the extinction coefficient, α, are available in Level 2A data. Given the known depth of the atmosphere layer in the ocean surface range bin, β and α may be used to correlate with residual range corrected Mie signal intensity that has not already been attributed to whitecap reflectance or subsurface reflection or specular reflection. It may be found that in cloud-free conditions, atmospheric constituents play a very minor (negligible?) role in the backscattered signal required to retrieve ocean surface wind speed.

It also needs to be considered that the radiation emanating from the surface bin is attenuated in the atmosphere on its way to the satellite receiver, depending on the concentrations and optical properties of the atmospheric constituents (e.g., aerosols, droplets, air molecules, …).

4 GEOPHYSICAL MODEL FUNCTION AND WIND INVERSION

In [2010], Li et al. discussed a framework to analyse the ultraviolet (355 nm) sea surface reflectance from an airborne Doppler Lidar. It has been indicated that the near surface returns are dominated by the reflectance of the surface and subsurface. In fact, Li et al. [2010] compared modelled return contributions and experimental data from an airborne field campaign in November 2007. The models used were based on earlier theoretical work of, e.g., Menzies et al. 1998], Flamant et al. [1998], Monahan and O'Muircheartaigh [1986], as well as Koepke [1984]. In short, to sketch the modelled dependencies, Menzies et al. [1998] expressed the total ocean water light reflectance as:

$$R = R_{wc} + (1 - W)R_s + (1 - R_{wc})R_U$$

Equation 4: Total surface reflectance.

R	Total reflectance	
R_s	Specular (surface) contribution	
$R_{wc} = W \cdot R_{wc,eff} \frac{\cos\theta}{\pi}$	Whitecap contribution	
$R_{wc,eff}$	Effective whitecap contribution	Constant
R_U	Subsurface (underwater) contribution	
θ	Off-nadir angle	Look angle
W	White caps coverage	Fraction

Note: *The model framework and comparisons of Li et al. [2010], see section* ***Error! Reference source not found.****, form the starting point of the wind speed retrieval approach. Furthermore, besides the more complex modelling already indicated in this work, also more recent achievements will be taken into consideration. For example, Josset et al. [2010] rewrite the total reflectance (Equation 4:* Total surface reflectance*as a bidirectional reflectance distribution function (BRDF) which is a function of the incidence angle and reflection angle. This may lead to more accurate description of the subsurface return contributions.*

4.1

White capping

The whitecap coverage W is modelled to be dependent on a higher power of the windspeed and, according to Monahan and O'Muircheartaigh [1986], an exponential dependence on the atmospheric stability:

$$W = 1.95 \cdot 10U^{2.25}\, e^{-0.0861\Delta T}$$

Equation 4: White cap coverage as a function of wind speed and atmospheric stability.

U	Surface wind speed (10m)	
$\Delta T = T_a - T_w$	The surface air-water temperature difference	

Firstly, the whitecap contribution R_{wc} itself is proportional to the whitecap fraction and a constant effective contribution as a Lambertian reflector, weighted with the observation angle.

Specular Reflection

4.2 The surface specular reflection R_s is originating from areas not covered with whitecaps and depends on the small wave facets (capillary and capillary-gravity waves). These facets are statistically described in terms of the wave slope variance. Cox and Munk [1954] modelled the wave slope variance σ^2 to be linearly dependent on the surface wind speed U. Other effects potentially affecting specular reflection such as surface films are not considered herein.

Next, Menzies et al. [1998], assuming surface wave isotropy, modelled the surface specular reflection R_s as

$$R_s = \frac{\rho}{2\pi\sigma^2(U)}\, e^{-\frac{\tan^2\theta}{\sigma^2(U)}}$$

Equation 5: Specular surface reflectance.

ρ	Fresnel reflectance	0.0219
σ	Mean square slope	

4.3

More complex wave slope variance models take e.g. the surface wave anisotropy (wind direction) into account.

Subsurface Reflection

Finally, the subsurface reflectance is again weighted with the off-nadir angle and a nadir term $R_{U,0}$ based on water volume scattering modelling, 'ocean colour' modelling, see e.g., Morel and Prieur [1977]:

$$R_U = R_{U,0}\frac{\cos\theta}{\pi}$$

Equation 6: Subsurface reflectance.

When crossing the air-sea interface, the unidirectional Lidar light beam is redistributed over a larger solid angle inside the water body: the rougher the sea surface, the wider the solid angle. However, since the distribution of the ocean surface facets can be assumed static for the short duration of the Lidar pulse, only strictly backscattered radiation can reach the receiver without undergoing a further scattering process. In other words, all single scattered photons reaching the receiver from the ocean subsurface have undergone backscattering at almost exactly 180°. In addition, multiple scattering processes will contribute to the subsurface returns, especially in low absorbing waters, but they will on average also involve a strong backscattering component.

Consequently, the backscattering efficiency of oceanic particles has a major influence on the intensity of the lidar sub-surface returns: the stronger the backscattering, the higher the subsurface signal. This means that sub-surface returns strongly increase with increasing presence of particulate material which makes ocean waters characterised by high and variable loads of phytoplankton or sediments a difficult choice for the proposed retrieval of the wind speed as it will be nearly impossible to estimate their contributions accurately enough to allow for a meaningful correction of the subsurface contribution.

On the other hand, strong absorption at the target wavelength of 355 nm will lead to reduced subsurface contributions. While pure sea water itself is only weakly absorbing at 355 nm, the absorption by coloured dissolved organic matter (CDOM) can be significant in CDOM-rich waters, making such waters very dark in the UV and blue spectral ranges.

The subsurface oceanic contribution to the surface bin can be either estimated from direct reflectance measurements or from radiative transfer (RT) calculations, requiring information on the absorption coefficient and volume scattering function of the surface water layer. Due to the inherent predominant contribution of backscattering from angles very close to 180°, the RT codes potentially applied for such calculations must perform well in this angular range, such as MC codes based on Monte Carlo methods, for example SMART-G.

The availability of reference data, preferably from in situ observations, for subsequent evaluation of the surface wind retrievals should also be taken into account for the test area selection process. **Error! Reference source not found.** designates areas representative of the three scenarios listed above.

At this point, it should be noted that observations of the subsurface reflectance and other optical parameters are relatively scarce at the ALADIN wavelength of 355 nm. The reason for this is that ocean colour retrieval methods are typically applied in the visible and near-infrared due to the difficulties of accurately estimating the atmospheric contribution to the top-of-atmosphere (TOA) signal in the UV.

Radiative transfer calculations may contribute to closing this knowledge gap, which will be elaborated at a later stage, if needed.

$$R_{U,0} = 0.088$$

4.4 Functional sensitivities

4.4.1 Whitecap fraction

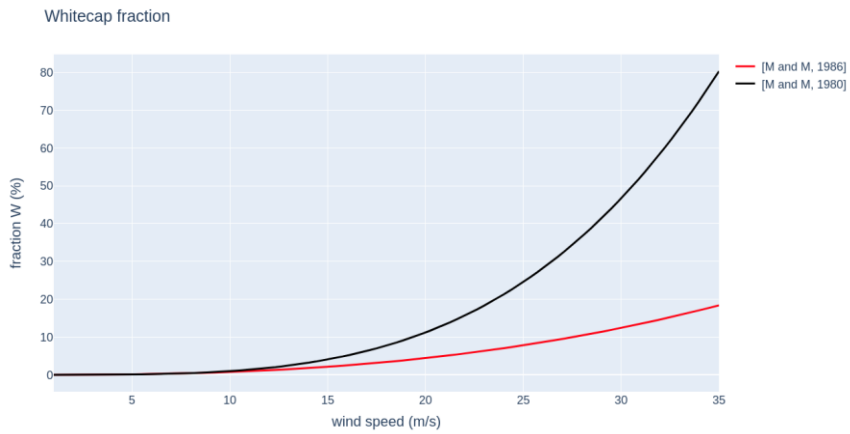

4.4.2 Relative total reflectance contributions

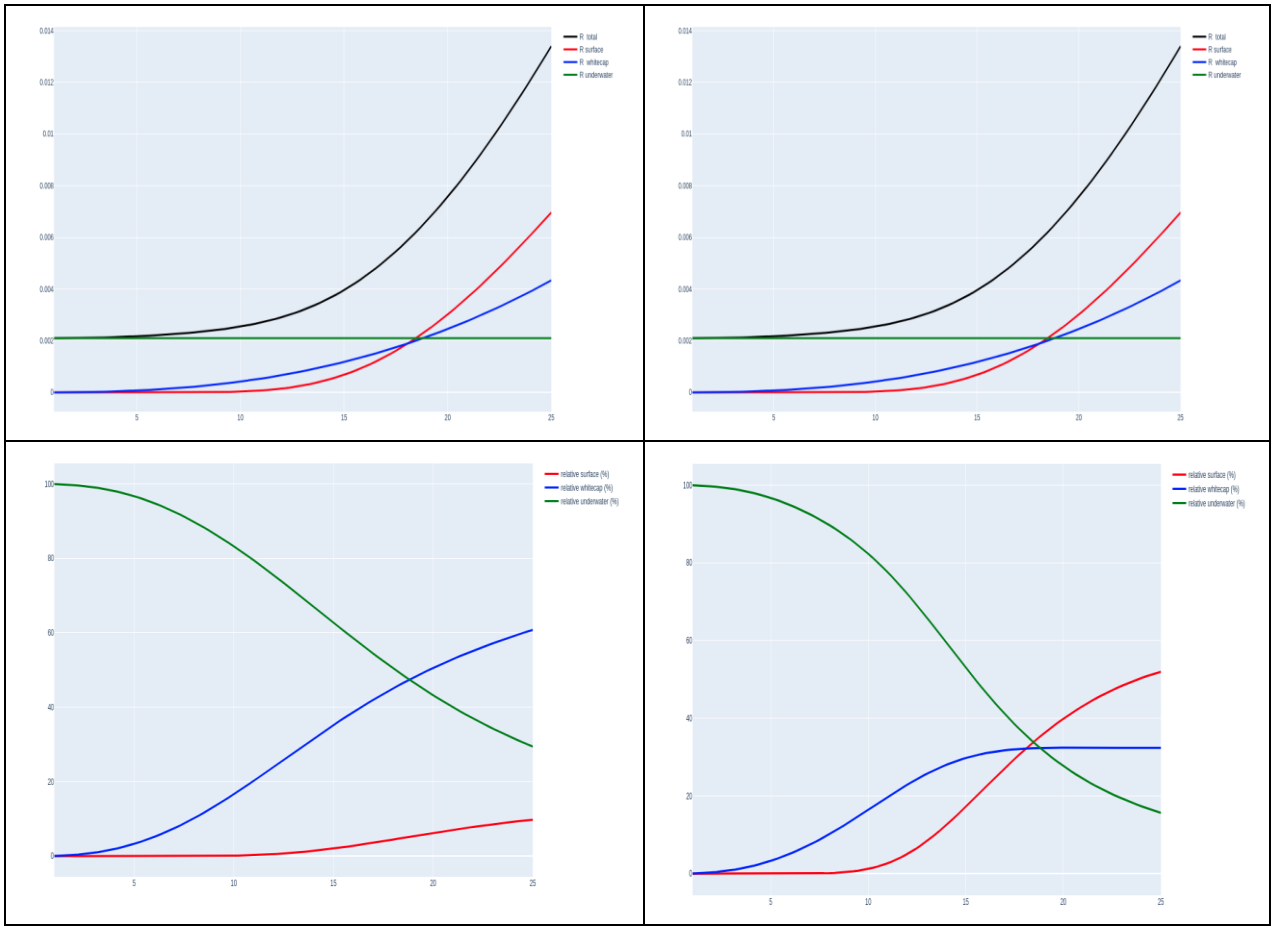

4.5

Wind inversion

Minimisation is executed using a Brent algorithm (as readily available. In python3 scipy)

bracketting. finding minima and

stopping criteria for the minimization will be investigated during this project.

The complex dependence of modelled reflectivity, $R(U)$, on wind speed may produce a solution space with multiple local minima, so care will be needed to ensure that retrieved wind speeds are not physically unrealistic owing

5 CALIBRATION AND VALIDATION

5.1 Test areas

From the retrieval and calibration/validation considerations presented above in sections 2.4 and 5, it follows that the identification of suitable areas is of crucial importance for both developing and applying the proposed method: In order to allow for a meaningful retrieval, the contributions from atmosphere and sub-surface must either be small as compared to the return from the ocean surface or they need to be estimated with sufficient accuracy. We therefore envisage the following three scenarios for developing the proposed surface wind retrieval:

1. "**Deep blue ocean**": Ocean areas of stable and known subsurface reflectance.
2. "**High winds**": Ocean areas frequently affected by high wind conditions.
3. "**Dark ocean**": Ocean areas characterised by low subsurface reflectance.

5.2 Collocations with wind data

5.2.1 Collocation with surface wind data.

The main source of ocean surface wind data for cal/val purposes are the level 2 scatterometer data from the ASCAT missions (A, B and C). These data are available from the EUMETSAT Ocean and Sea Ice Satellite Application Facility (OSISAF) at KNMI under https://scatterometer.knmi.nl/osisaf/.

In the ASCAT products, essential Level 1B information (e.g. the sigma0's Kp) is propagated into the Level 2 products to enhance the understanding of the scatterometer wind measurement.

The base-line Aeolus L2B observation size is about 86 km along track. [CAL/VAL REQ], therefore spatially there is good co-location with the OSI SAF ASCAT 25 km products. Also, the coastal ASCAT products may be taken into consideration, perhaps with an additional averaging applied. The global distribution of Aeolus-ASCAT collocations will be assessed *a priori* (before major download processing) to optimize the effort to create the data pool.

5.2.2 Collocation with aux_met

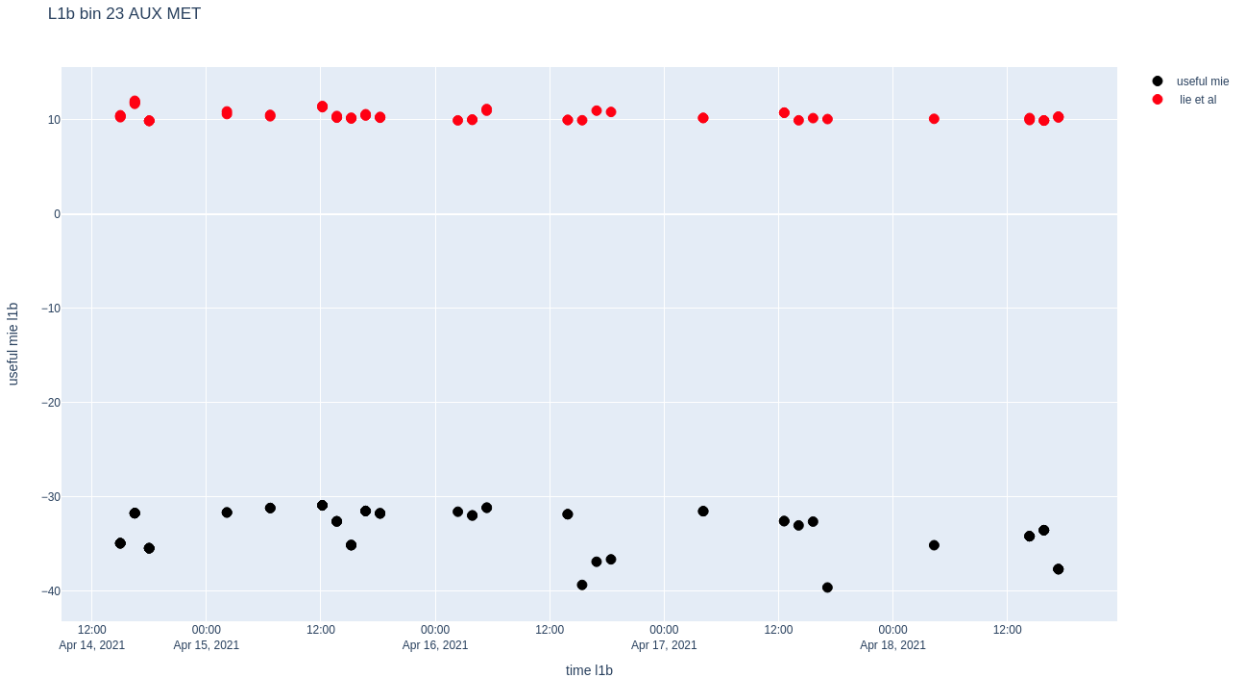
L1b bin 23 AUX MET
useful mie
lie et al
useful mie l1b
10
0
−10
−20
−30
−40
12:00
Apr 14, 2021
00:00
Apr 15, 2021
12:00
00:00
Apr 16, 2021
12:00
00:00
Apr 17, 2021
12:00
00:00
Apr 18, 2021
12:00
time l1b

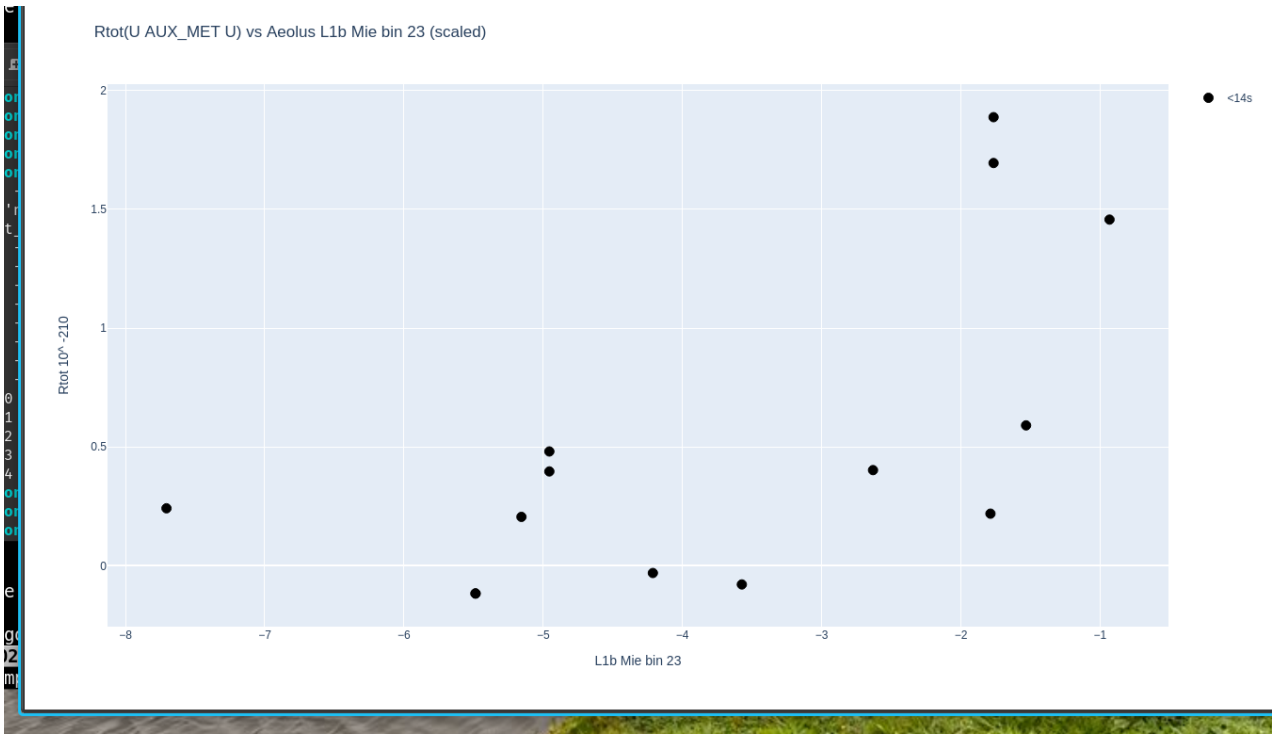
Rtot(U AUX_MET U) vs Aeolus L1b Mie bin 23 (scaled)
<14s
Rtot 10^-210
2
1.5
1
0.5
0
−8
−7
−6
−5
−4
−3
−2
−1
L1b Mie bin 23

5.2.3 Collocation with Ocean Colour data

For the assessment of the subsurface contribution in the GMF, the Aeolus-ASCAT data shall be additionally collocated with Ocean Colour data. Our main OC source will be the OLCI products. Recently, on 16. Feb 2021, a new release of intervalidated OLCI data have been published. under the name 'collection 3': https://www-cdn.eumetsat.int/files/2021-02/S3%20PN-OLCI-L2M_003_00%20-%20Sentinel-3%20Product%20Notice%20–%20OLCI%20Level-2%20Ocean%20Colour.pdf.

Scenario 1: Deep blue ocean (Box E)

5.3

This blue colour is well visible from space. Satellite observations can thus be used to identify such hyperoligotrophic waters (Figure 1).

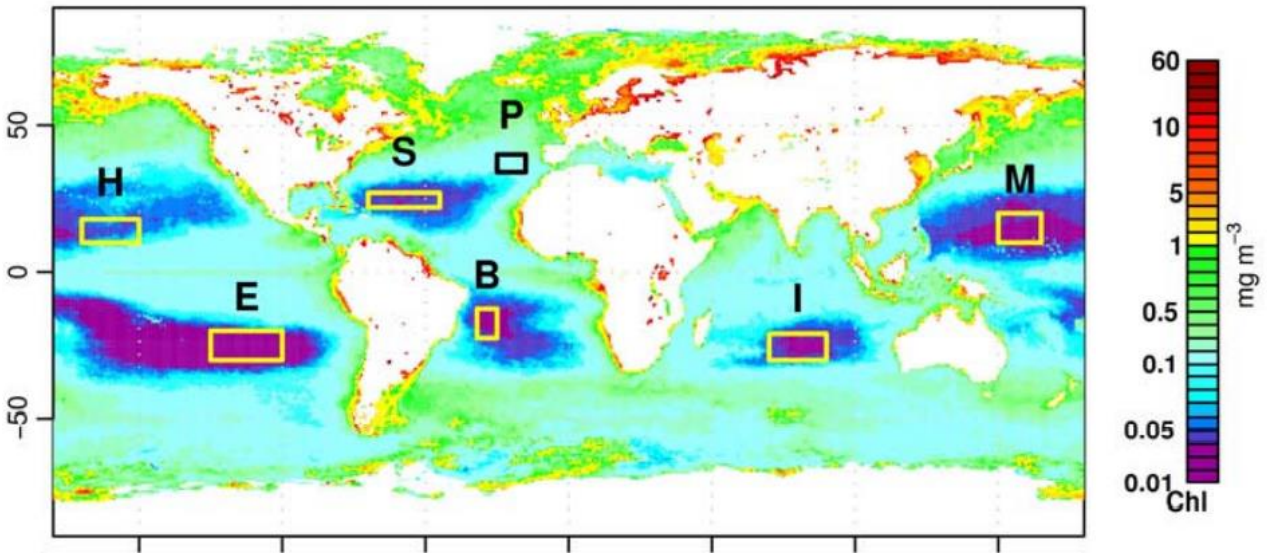

Figure 1: Chlorophyll concentration [Chl] (mg m^{-3}), annual composite (year 2006) of SeaWiFS data for the global ocean. The rectangle E (for Easter Island) is located in the South Pacific Gyre. Source: Morel et al. [2010].

The clearest natural waters in the world are found in the cores of the large subtropical anticyclonic gyres. This clarity is caused by extremely low concentrations of both phytoplankton and coloured dissolved organic matter (CDOM) and results in a specific deep blue colour (**Error! Reference source not found.**) for these hyperoligotrophic waters due to enhanced reflectance in the blue, violet, and UV [Morel et al., 2010].

The biggest subtropical anticyclonic gyre on Earth is located in the Southern Pacific Ocean between roughly 15° - 30° South and 100° - 150° West. This area, the South Pacific Gyre (SPG), contains the most oligotrophic waters on Earth, covers more than 2 million square kilometres, and has additionally been comparably well investigated due to a number of dedicated oceanographic campaigns (see below). It is proposed herein as one site for retrieval development.

Its main advantage for retrieval development lies in the fact that the subsurface reflection, while not small in the UV, is very constant over space and time inside the hyperoligotrophic core of the gyre. It thus forms a stable reflectance background against which wind speed related reflectance patterns should become visible. In cases of known low windspeed conditions, the absolute subsurface background reflectance may even be directly estimated from the ALADIN returns. Alternatively, it may be derived from measured reflectance spectra or from appropriately configured radiative transfer simulations.

Figure 2: Reflectance spectra (ca. 350 to 700 nm) of the clearest waters in the South Pacific Gyre in the near surface layer. Additional shown (dotted) is a reflectance spectrum from Crater Lake in Oregon [Tyler and Smith, 1970], a very clear lake of volcanic origin. Source: Morel et al. [2007].

The optical properties of the hyperoligotrophic waters in the SPG have been studied in the context of dedicated oceanographic campaigns, for example the *Biogeochemistry and Optics South Pacific Experiment* (BIOSOPE)[1], including in situ measurements of the apparent and inherent optical properties (AOPs and IOPs) in the UV spectral domain. Of special relevance to the proposed sea surface wind retrieval are the surface reflectance measurements taken by Morel et al. [2017], see Figure 2.

To this date, there is still no unanimous agreement on the optical properties of pure water in the UV (as it is very difficult to obtain water of the required purity without any substantial CDOM contribution). Reflectance measurements such as those shown in Figure 2 have been used by Morel et al. (2007) to derive the absorption coefficient of pure water in the UV. Such knowledge on the absorption (and scattering) of pure water is important if one wants to simulate the sub-surface reflectance using radiative transfer models.

5.3.1 Scenario 2: High winds

The “High Winds” scenario aims at exploiting conditions where high wind speeds occur over oligotrophic waters of possibly known optical properties. This would allow to estimate the subsurface contribution with a relatively good accuracy and at the same time ensure a strong signal from the ocean surface.

5.3.2 Scenario 3: Dark ocean

6 SUMMARY